

Antiferromagnetism and chiral d -wave superconductivity from an effective t - J - D model for twisted bilayer graphene

Xingyu Gu,^{1,2} Chuan Chen,^{2,3} Jia Ning Leaw,² Evan Laksono,^{2,4} Vitor M. Pereira,^{1,2} Giovanni Vignale,^{2,5,6} and Shaffique Adam^{1,2,5}

¹*Department of Physics, National University of Singapore, 117542, Singapore*

²*Centre for Advanced 2D Materials and Graphene Research Centre, National University of Singapore, 117546, Singapore*

³*Max-Planck Institute for the Physics of Complex Systems, 01187 Dresden, Germany*

⁴*Department of Physics, Stanford University, Stanford, California 94305, USA*

⁵*Yale-NUS College, 16 College Avenue West, 138527, Singapore*

⁶*Department of Physics and Astronomy, University of Missouri, Columbia, Missouri 65201, USA*



(Received 12 September 2019; revised manuscript received 6 January 2020; accepted 20 April 2020; published 11 May 2020)

We derive an effective tight-binding model that captures, in real space and with only two parameters, the dominant Coulomb interactions and superconducting pairing near half-filling of magic-angle twisted bilayer graphene. We show that, in an antiferromagnetic Mott insulating ground state with intervalley coherence, magnetic fluctuations and doping mediate superconducting pairing. We find the pairing wave function to have chiral d -wave symmetry and obtain a self-consistent mean-field phase diagram in line with experiments on the doping-induced insulator-to-superconductor transition. We further reveal the existence of chiral Majorana edge modes implied by the nontrivial pairing symmetry, which establishes twisted bilayer graphene as a potential platform for topological superconductivity. This effective model opens the door to systematic scrutiny of the competition between correlated states in this system.

DOI: [10.1103/PhysRevB.101.180506](https://doi.org/10.1103/PhysRevB.101.180506)

Introduction. Correlated insulating phases and unconventional superconductivity (SC) have been recently observed in twisted bilayer graphene (tBG) near the magic angle $\theta \approx 1.1^\circ$ [1–3], igniting a surge of interest due to the similarity of its phase diagram and that of high- T_c superconductors. Theoretical proposals emerged since to address the nature of those phases from either a weak- or strong-coupling limit of the electronic interactions [4–21]. In weak coupling, van Hove singularities and Fermi surface nesting [22,23] suggest the possibility of strong particle-hole fluctuations that can lead to an insulating phase and SC upon doping [5–7,10]. On the other hand, the multiple insulating phases observed experimentally [3] favor strong coupling to be more appropriate.

It has been shown that a minimal tight-binding (TB) Hamiltonian must consist of two orbitals, of p_x and p_y symmetry, per site of the emergent honeycomb spanned by the regions of perfect AB and BA stacking [blue and red sites in Fig. 1(a)] [9,11–13,24]. In this view, to each valley $\pm K$ one associates a TB with a single $p_x \pm ip_y$ orbital on each site, thus generating a two-band model per valley [11–13]. However, there is topological obstruction to describe individual valleys by independent TB Hamiltonians while maintaining the valley $U(1)$ symmetry [11]. Although this would force the four-band model as the minimal description, phenomenological considerations and Hartree-Fock calculations suggest that the valley symmetry may be broken spontaneously above the Mott and SC transition temperatures [11].

In this scenario, the symmetry-broken state is characterized by an intervalley coherence (IVC, where the valley pseudospin acquires a polarization in the xy plane), and two pairs of bands can split as schematically illustrated in Fig. 1(b) [11]. The Fermi level at a filling of two electrons per moiré unit cell (half filling) is then at the Dirac points of the lower band pair. The system is then semimetallic without further symmetry breaking. The experimentally observed insulating and SC phases are assumed to arise in this IVC state. This picture is consistent with experimental Landau level degeneracy near half filling [1–3] as well as experiments that suggest spin-singlet Mott-like behavior in the insulating phase [1].

To adequately incorporate Coulomb interactions, one must consider that the trilobed shape of Wannier functions [see Fig. 1(a)] generates a cluster interaction, which leads to an extended Hubbard model [11,12,24]. Reference [17] explored its possible symmetry-broken phases using quantum Monte Carlo and, as in monolayer graphene, the ground state in the strong-coupling limit has antiferromagnetic (AFM) order [25,26]. Reference [24], on the other hand, suggested a ferromagnetic ground state by calculating the exchange integrals explicitly.

In this Rapid Communication, we adopt the IVC scenario and concentrate on the vicinity of half filling. We derive an effective model that, with minimal parameters, captures the dominant AFM coupling and fluctuation-induced SC pairing in tBG at the magic angle, which is the “ t - J - D model” we

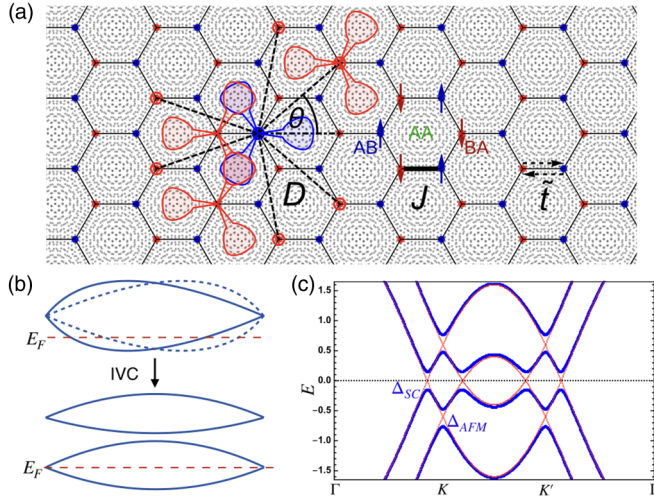


FIG. 1. (a) Blue/red dots mark the places with perfect AB/BA stacking in the moiré pattern, which define a honeycomb lattice. The trilobed forms illustrate the shape of the Wannier functions. The renormalized hopping, antiferromagnetic coupling, and pairing strength are denoted as \tilde{t} , J , and D , respectively, and vertical arrows represent the short-range AFM order. (b) Intervalley coherence (IVC) order splits the low-energy four-band sector into two pairs; at half filling, the Fermi level is at the lowest Dirac crossings. (c) Quasiparticle dispersion along the Γ - K - K' - Γ line in the moiré Brillouin zone when both AFM and SC gaps are finite and the system is doped away from half filling (noninteracting spectrum in red). The SC gap opens at the Fermi level (dashed line) while the AFM gap remains at the Dirac point.

introduce here. It is governed by the effective Hamiltonian $H = H_{\tilde{t}} + H_J + H_D$, where

$$H_{\tilde{t}} \equiv -\tilde{t} \sum_{\langle ij \rangle, \alpha} a_{i\alpha}^\dagger b_{j\alpha} + \text{H.c.}, \quad (1a)$$

$$H_J \equiv J \sum_{\langle ij \rangle} \vec{S}_i \cdot \vec{S}_j, \quad (1b)$$

$$H_D \equiv -D \sum_{\langle\langle ij \rangle\rangle} h_{ij}^\dagger h_{ij}. \quad (1c)$$

The effective hopping \tilde{t} takes into account the strong renormalization of the single-particle bandwidth due to electron correlations (see Supplemental Material [27] for the order of \tilde{t}). It describes the itinerancy of electrons among nearest-neighbor sites i, j of the honeycomb lattice defined by the AB/BA regions in the moiré lattice, a and b are the electron operators on each sublattice, and α indicates spin. The term H_J describes an AFM exchange interaction between nearest-neighbor spins, \vec{S}_i , and H_D represents the fluctuation-induced pairing with $\langle\langle ij \rangle\rangle$ indicating third neighbors not sharing an hexagon, such as the blue and red pairs represented in Fig. 1(a). $h_{ij} \equiv a_{i\uparrow} b_{j\downarrow} - a_{i\downarrow} b_{j\uparrow}$ is the intersublattice singlet operator. We emphasize that, unlike in the approach to cuprates or pnictides [28], in this model the SC pairing couples not the nearest but remote neighbors, as schematically shown by the dashed lines in Fig. 1(a).

In addition to deriving the effective model in Eq. (1), we extract the implication that pairing should be chiral with

$d + id$ symmetry, which tallies with conclusions from other models [4,6,8,14,15,19,21]. We also show that the model-derived phase diagram agrees with the experimental sequence of transitions as a function of doping away from half filling.

Effective model. We start from the real-space Hamiltonian $H = H_t + H_U$ on the honeycomb lattice spanned by the centers of the Wannier functions [see Fig. 1(a)]. As there is no symmetry obstruction to building a two-band TB model in the IVC state [11], we consider a single Wannier orbital per site of the emergent honeycomb lattice. Hence

$$H_t \equiv -t \sum_{\langle ij \rangle, \alpha} a_{i\alpha}^\dagger b_{j\alpha} + \text{H.c.}, \quad (2a)$$

$$H_U \equiv U \sum_R (Q_R - 2)^2. \quad (2b)$$

Here, t is the *bare* hopping (i.e., the hopping in the absence of interactions), R marks the position of each hexagon's center, U sets the strength of the repulsive interactions, and $Q_R \equiv \sum_{i \in \square} \sum_{\alpha} \frac{n_{i\alpha}}{3}$ is the charge located at that position. The unusual form of the interaction H_U contrasts with the more conventional on-site Hubbard interaction, which would be overly simplistic here. This happens because symmetry imposes the Wannier functions associated with the flat bands to have a trilobed shape centered on the AB/BA sites [9,11–13]. As illustrated in Fig. 1(a), each Wannier function is shared by the three adjacent hexagons and its lobes extend up to the centers of those hexagons. The electronic density is therefore peaked at the positions of the dual triangular lattice, which is seen experimentally [29]. This results in the overlap of 3, 2, or 1 lobes when considering, respectively, the interaction between electrons on the same site, nearest-neighbor (NN), next NN (NNN), and third NN on a given hexagon. Correspondingly, the ratios of the repulsion from same site to third NN is 3:2:1:1 [12].

As the interaction is still larger on site than among NN, an AFM coupling $J \sim t^2/U$ arises to leading order in perturbation theory for $U \gg t$ [30], which defines our term H_J in Eq. (1b). This exchange term is further validated by the discovery of AFM order in quantum Monte Carlo calculations [17]. Furthermore, we note that the puzzle of Landau level degeneracy reduction seen in magnetic quantum oscillation experiments [1–3] can be qualitatively explained in our model; considering that the saddle points lie extremely close (≈ 0.1 meV) to the moiré Dirac point energies [12], one indeed expects [31–34] an experimental degeneracy of 2 (spin) at half-filling within IVC, as observed.

Unlike in cuprates and iron pnictides [28], in tBG one expects NN pairing to be inefficient due to the strong repulsion (governed by H_U) between electrons sharing a given hexagon. Therefore, we consider the pairing between the closest electrons not coupled by H_U . These are the six sites marked by the red disks in Fig. 1(a), which lie closest to the site highlighted in blue. We now show the basic physics of how AFM fluctuations mediate an effective pairing between electrons at these sites (see Supplemental Material [27] for a more detailed treatment).

Decoupling the AFM order parameter $\vec{m}_i \equiv \frac{(\vec{S}_a - \vec{S}_b)}{2}$ in the electronic interaction leads to a local magnetic coupling $H_i = \lambda \vec{m}_i \cdot \vec{\sigma}_{\alpha\beta} (a_{i\alpha}^\dagger a_{i\beta} - b_{i\alpha}^\dagger b_{i\beta})$, where $\lambda \sim J$ is the coupling

strength [35]. Here we consider the effect of magnetic fluctuations in the absence of long-range AFM order. The intersublattice effective electron-electron interaction can be obtained by integrating out the spin fluctuations, and reads

$$H_{ij} = \lambda^2 \chi_{ij} \vec{\sigma}_{\alpha\beta} \cdot \vec{\sigma}_{\gamma\delta} a_{i\alpha}^\dagger a_{i\beta} b_{j\gamma}^\dagger b_{j\delta}. \quad (3)$$

It arises in an approximation that neglects retardation effects, where $\chi_{ij} \propto g^{-1} e^{-R_{ij}/\xi}$ is the static spin susceptibility, with R_{ij} the distance between moiré unit cells i and j , ξ the magnetic correlation length, and g the spin stiffness (see Supplemental Material [27] for the meaning of g). One sees that H_{ij} is attractive for antiparallel spins ($\alpha = \beta = -\gamma = -\delta$), and should hence support singlet SC [36], in line with experimental observations [2]. The pairing strength in Eq. (1c) is determined by $D \sim \lambda^2 \chi_{ij}$ and will be significant as long as spin fluctuations are strong (ξ_{ij} is large). Since the spin stiffness is controlled by J , D should also be of order J . Moreover, similar arguments show that the intrasublattice interaction between antiparallel spins is repulsive. Such a staggered “attractive-repulsive” profile is similar to cuprates, where it arises from Fermi surface nesting [36–38]. Even though these similarities provide universal points of contact between tBG and high- T_c materials, we underline the unique features of the t - J - D model in Eq. (1), where AFM interactions in (1b) are governed by NN exchange, as in a conventional t - J model [39–41], whereas fluctuation-induced pairing (1c) is relevant only among more distant sites.

In order to establish the basic phenomenology implied by this model, we investigated its phase diagram at the mean-field level. In the remainder, we study the ground state of Hamiltonian (1) considering only pairing among sites such as those connected by the dashed lines in Fig. 1.

Pairing symmetry. Before studying the interplay between AFM and SC phases, we tackle the case with $J = 0$ in Eq. (1) to identify the symmetry of the dominant pairing instability. Decoupling the interaction in Eq. (1c) at the mean-field level we have

$$\begin{aligned} H_D^{MF} &= \sum_{i,\mathbf{a}} -\Delta_{\mathbf{a}} h_{i,i+\mathbf{a}}^\dagger - \Delta_{\mathbf{a}}^* h_{i,i+\mathbf{a}} + \frac{6N}{D} |\Delta|^2 \\ &\simeq - \sum_{\mathbf{k}} D_{\mathbf{k}} c_{\mathbf{k}\uparrow}^\dagger c_{-\mathbf{k}\downarrow}^\dagger + \text{H.c.} + \frac{6N}{D} |\Delta|^2, \end{aligned} \quad (4)$$

where $\Delta_{\mathbf{a}} \equiv D \langle h_{i,i+\mathbf{a}} \rangle$ denotes the pairing between electrons at i and $i + \mathbf{a}$, and \mathbf{a} represents the six vectors connecting blue and red sites in Fig. 1. In the second line, c is the conduction-band fermion operator and $D_{\mathbf{k}} \equiv \sum_{\mathbf{a}} \Delta_{\mathbf{a}} \cos(\mathbf{k} \cdot \mathbf{a} - \phi_{\mathbf{k}})$ defines the SC gap, with $\phi_{\mathbf{k}} \equiv \arg(\sum_{\delta} e^{i\mathbf{k} \cdot \delta})$ and δ being the three vectors connecting the NN sites. This result (4) retains only intra-conduction-band pairing terms, since these are the most important at finite chemical potential which is the situation where SC is observed experimentally (see Supplemental Material [27] for more details of the calculation).

The pairing symmetry in the ground state has been obtained by the self-consistent mean-field solution using the Hamiltonian (4). The pairing function is written as $\Delta_{\mathbf{a}} = \Delta f(\theta_{\mathbf{a}})$, where $\theta_{\mathbf{a}}$ is the angle between bond \mathbf{a} and the x axis [see θ in Fig. 1(a)]. We use $f_s(\theta) = 1$, $f_{d_{x^2-y^2}}(\theta) = \cos(2\theta)$, $f_{d_{xy}}(\theta) = \sin(2\theta)$, and $f_{d+id}(\theta) = e^{i2\theta}$

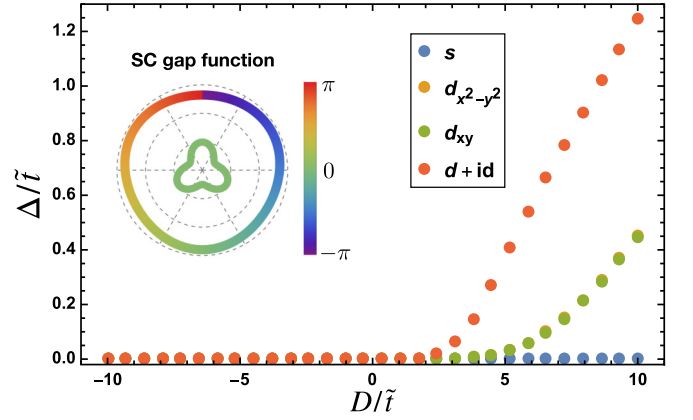


FIG. 2. Solution of gap equation (5) for different pairing symmetries. The s -wave order parameter is always negligibly small, while the other symmetries develop order at finite D . The solutions for $d_{x^2-y^2}$ and d_{xy} are degenerate, which is protected by symmetry. The critical pairing (D_c) is smallest for $d + id$ symmetry. The inset shows the magnitude (radius) and phase (color) of the s and $d + id$ gap functions along a circle centered at the Dirac point with radius $k = 0.1/a$ when $\Delta_{\mathbf{a}} = 1$. The outer (inner) ring represents $d + id$ (s) symmetry. For visibility, the magnitude of the s -wave order parameter has been increased fivefold.

in our calculation. The quasiparticle spectrum is given by $E_{\mathbf{k}} = \pm \sqrt{(\epsilon_{\mathbf{k}} - \mu)^2 + |D_{\mathbf{k}}|^2}$, where μ is the chemical potential measured with respect to the Dirac points and $\epsilon_{\mathbf{k}} \equiv \tilde{t} \sqrt{3 + 2 \cos(\sqrt{3}k_y)} + 4 \cos(\frac{\sqrt{3}k_x}{2}) \cos(\frac{3k_x}{2})$ is the dispersion of free electrons in the emergent honeycomb lattice [42] (see Supplemental Material [27] for the calculation). By minimizing the energy, we obtain the gap equation:

$$\frac{1}{N} \sum_{\mathbf{k}} \frac{|\sum_{\mathbf{a}} f(\theta_{\mathbf{a}})|^2}{E_{\mathbf{k}}} = \frac{12}{D}, \quad (5)$$

where N is the number of unit cells. The solutions of this equation as a function of V for each symmetry are shown in Fig. 2, where we chose $\mu = 0.2\tilde{t}$ for illustration. For repulsive interaction ($D < 0$), there is obviously no SC at all. For attractive interactions ($D > 0$), while the s -wave order parameter remains zero for D up to 10, a d -wave emerges at a finite critical interaction, D_c . The case $d + id$ has both the smallest D_c and the largest magnitude at a given D , which implies the ground state should have $d + id$ symmetry. We can understand why $d + id$ is favored in relation to s -wave symmetry by inspecting the different gap functions in momentum space ($D_{\mathbf{k}}$) while setting the real-space amplitudes to $\Delta_{\mathbf{a}} = 1$ [28]. As the condensation energy is dominated by the opening of the SC gap at the Fermi surface, in the inset of Fig. 2 we show a polar representation of $D_{\mathbf{k}}$ along the circle centered at the Dirac point with radius $k = 0.1/a$ (a is the moiré lattice constant) for the cases of s and $d + id$ wave. This confirms directly that $D_{\mathbf{k}}^{(s)} \ll D_{\mathbf{k}}^{(d+id)}$ and, in addition, shows that the case $d + id$ displays a nontrivial winding phase of 2π around each moiré Dirac point (see Supplemental Material [27] for more information of $D_{\mathbf{k}}$). To reveal the nontrivial topology of the $d + id$ explicitly, we show the Bogoliubov quasiparticle spectrum in the superconducting phase with ribbon

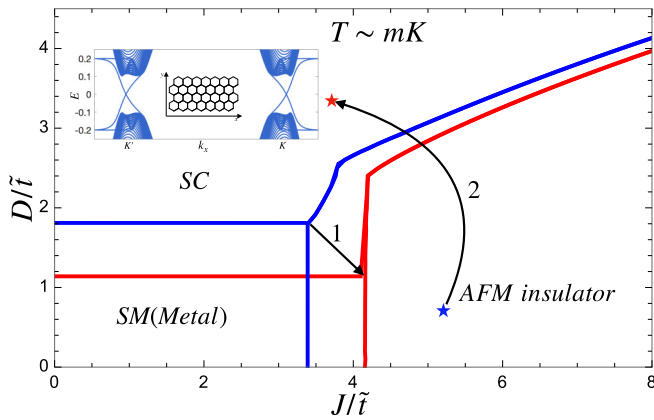


FIG. 3. Mean-field phase diagram for $\mu = 0$ (blue) and $\mu = 0.5$ (red). Cooper instability predicts SC ground states for arbitrarily weak attractive interactions, but the critical temperature becomes exponentially small when the interaction is too weak. To take into account we stipulate that the system is in the SC or in the AFM state only when the corresponding order parameter exceeds $0.01\tilde{t}$, which corresponds to a critical temperature of 2 mK—the lowest temperature accessible experimentally. Our phase diagram can be understood as being essentially the phase diagram at $T \sim \text{mK}$. The system is a semimetal in the weak-coupling region, an AFM insulator at large J , and SC at large D . Arrow 1 highlights the increase in J_c and decrease in D_c upon doping, while arrow 2 shows the transition from AFM state to SC observed experimentally when tuning chemical potential (see text). The inset shows the Bogoliubov quasiparticle spectrum in the superconducting phase with ribbon geometry.

geometry in the inset of Fig. 3 (see Supplemental Material [27] for more details). Two chiral Majorana modes are observed and they have a fingerprint of quantized Hall conductivity which may be detected in transport experiments similar to those of Ref. [43].

A similar $d + id$ SC phase is obtained in monolayer graphene if one considers only NN pairing [44,45]. Hence $d + id$ pairing is likely a robust feature of correlation-driven SC in honeycomb lattices in strong coupling. But, crucially, whereas in a monolayer the interaction is too weak ($U/t \sim 3.3$ [46,47]), in tBG, the quasiflat band drives the system into strong coupling making it an ideal platform to realize topological SC.

Parameters. A central aspect of the electronic structure of tBG is the extremely small value of the bare hoppings ($t \lesssim 1 \text{ meV}$ [1,12,13,48]) and the much larger interaction strength that justifies our strong-coupling approach ($U \approx 40 \text{ meV}$, using results of Ref. [12] and encapsulated in boron nitride; hence $U/t \gtrsim 40$). In turn, this leads to an estimate of the AFM exchange $J = 2t^2/U \approx 0.05 \text{ meV}$. Moreover, the effective hopping \tilde{t} that governs the electronic motion in the effective

Hamiltonian (1) is estimated in the Supplemental Material [27], Sec. S1, to be $\tilde{t} \sim J/3 \approx 17 \mu\text{eV}$. Consequently, since Fig. 2 shows $D_c/\tilde{t} \sim 2$, the stability of a SC phase requires only that the pairing strength D exceeds a few μeV . This is consistent with the facile observation of SC in experiments where tBG is slightly doped away from the half filled correlated insulator state [2].

Interplay of AFM and SC. Reinstating the AFM interaction ($J \neq 0$), we now probe the relative stability of the two phases according to the full Hamiltonian in Eq. (1). According to the discussion above, we consider only $d + id$ pairing symmetry. Figure 3 shows the mean-field phase diagram (see Supplemental Material [27] for the calculation), where the blue (red) lines were obtained for $\mu = 0$ ($\mu = 0.5\tilde{t}$). The system is (semi)metallic in weak coupling, where both D and J are small. From here, increasing J or D leads to a transition to either an AFM or SC state as expected. Arrow 1 highlights that departing from half filling stabilizes the SC phase at the expense of AFM order. SC is favored at higher densities because the AFM gap is pinned to the Dirac point, independent of μ . As a result, the energy gained by transitioning to the AFM state is maximum at half-filling but decreases with doping. In contrast, the SC gap lies at the Fermi level; the associated energy gain is operative at any μ and becomes more pronounced with doping because of the increase in Fermi surface. When $\mu = 0$, the transitions from SM to either the AFM or SC phases are continuous, while the AFM-SC transition is of first order; at finite chemical potential, the SM-AFM evolves to first order (see Supplemental Material [27] for details).

The phase diagram in Fig. 3 tallies with experiments: while tBG is insulating at half filling and low temperature, doping drives it to a SC state [1,2]. If $J/\tilde{t} \gtrsim 3.5$, our framework obtains indeed an insulator at half filling with a gap Δ_{AFM} , and should display AFM order. We note that Fig. 3 has been obtained with J , D , and μ as free, independent parameters. In reality, doping will have two consequences on the effective couplings: (i) a decrease of J/\tilde{t} since more carriers destabilize the effective exchange and increase the effective bandwidth [49]; (ii) an increase of D due to stronger magnetic fluctuations [cf., Eq. (3)] when departing from half filling [50]. These effects further facilitate the doping-induced transition from the insulating/AFM to the SC state, as schematically illustrated by arrow 2. To accommodate the extreme doping sensitivity of the insulating state seen experimentally, the diagram in Fig. 3 constrains J/\tilde{t} to be near 3–4. We expect the renormalized hopping to be $\tilde{t} \sim J/3$ near half filling, which places our predictions in line with experiments.

Acknowledgments. We thank N. Raghuvanshi for helpful discussions. This work was supported by the Singapore Ministry of Education Grants No. MOE2017-T2-1-130 and No. MOE2017-T2-2-140.

- [1] Y. Cao, V. Fatemi, A. Demir, S. Fang, S. L. Tomarken, J. Y. Luo, J. D. Sanchez-Yamagishi, K. Watanabe, T. Taniguchi, E. Kaxiras *et al.*, *Nature (London)* **556**, 80 (2018).
 [2] Y. Cao, V. Fatemi, S. Fang, K. Watanabe, T. Taniguchi, E. Kaxiras, and P. Jarillo-Herrero, *Nature (London)* **556**, 43 (2018).

- [3] M. Yankowitz, S. Chen, H. Polshyn, Y. Zhang, K. Watanabe, T. Taniguchi, D. Graf, A. F. Young, and C. R. Dean, *Science* **363**, 1059 (2019).
 [4] C. Xu and L. Balents, *Phys. Rev. Lett.* **121**, 087001 (2018).
 [5] H. Isobe, N. F. Q. Yuan, and L. Fu, *Phys. Rev. X* **8**, 041041 (2018).

- [6] C.-C. Liu, L.-D. Zhang, W.-Q. Chen, and F. Yang, *Phys. Rev. Lett.* **121**, 217001 (2018).
- [7] E. Laksono, J. N. Leaw, A. Reaves, M. Singh, X. Wang, S. Adam, and X. Gu, *Solid State Commun.* **282**, 38 (2018).
- [8] D. M. Kennes, J. Lischner, and C. Karrasch, *Phys. Rev. B* **98**, 241407(R) (2018).
- [9] N. F. Q. Yuan and L. Fu, *Phys. Rev. B* **98**, 045103 (2018).
- [10] Y.-Z. You and A. Vishwanath, *npj Quantum Mater.* **4**, 16 (2019).
- [11] H. C. Po, L. Zou, A. Vishwanath, and T. Senthil, *Phys. Rev. X* **8**, 031089 (2018).
- [12] M. Koshino, N. F. Q. Yuan, T. Koretsune, M. Ochi, K. Kuroki, and L. Fu, *Phys. Rev. X* **8**, 031087 (2018).
- [13] J. Kang and O. Vafek, *Phys. Rev. X* **8**, 031088 (2018).
- [14] H. Guo, X. Zhu, S. Feng, and R. T. Scalettar, *Phys. Rev. B* **97**, 235453 (2018).
- [15] T. Huang, L. Zhang, and T. Ma, *Sci. Bull.* **64**, 310 (2019).
- [16] J. F. Dodaro, S. A. Kivelson, Y. Schattner, X. Q. Sun, and C. Wang, *Phys. Rev. B* **98**, 075154 (2018).
- [17] X. Y. Xu, K. T. Law, and P. A. Lee, *Phys. Rev. B* **98**, 121406(R) (2018).
- [18] L. Zou, H. C. Po, A. Vishwanath, and T. Senthil, *Phys. Rev. B* **98**, 085435 (2018).
- [19] M. Fidrysiak, M. Zegrodnik, and J. Spałek, *Phys. Rev. B* **98**, 085436 (2018).
- [20] A. Thomson, S. Chatterjee, S. Sachdev, and M. S. Scheurer, *Phys. Rev. B* **98**, 075109 (2018).
- [21] X.-C. Wu, C.-M. Jian, and C. Xu, *Phys. Rev. B* **99**, 161405(R) (2019).
- [22] R. Bistritzer and A. H. MacDonald, *Proc. Natl. Acad. Sci. USA* **108**, 12233 (2011).
- [23] J. M. B. Lopes dos Santos, N. M. R. Peres, and A. H. Castro Neto, *Phys. Rev. Lett.* **99**, 256802 (2007).
- [24] K. Seo, V. N. Kotov, and B. Uchoa, *Phys. Rev. Lett.* **122**, 246402 (2019).
- [25] H.-K. Tang, J. Leaw, J. Rodrigues, I. Herbut, P. Sengupta, F. Assaad, and S. Adam, *Science* **361**, 570 (2018).
- [26] Although the AFM insulating phase in this model has the same origin as in the monolayer, the cluster interaction reduces the effective on-site repulsion, which might explain the small gap of the insulating phase observed experimentally. Unlike in monolayer graphene, the Monte Carlo results also found a Kekulé valence bond solid phase at intermediate coupling, but this is not germane to our considerations here.
- [27] See Supplemental Material at <http://link.aps.org/supplemental/10.1103/PhysRevB.101.180506> for the details of renormalized hopping, fluctuation induced pairing, mean field analysis, superconductivity gap and chiral Majorana modes.
- [28] J. Hu, *Sci. Bull.* **61**, 561 (2016).
- [29] S. Huang, K. Kim, D. K. Efimkin, T. Lovorn, T. Taniguchi, K. Watanabe, A. H. MacDonald, E. Tutuc, and B. J. LeRoy, *Phys. Rev. Lett.* **121**, 037702 (2018).
- [30] P. W. Anderson, *Phys. Rev.* **79**, 350 (1950).
- [31] M.-Y. Choi, Y.-H. Hyun, and Y. Kim, *Phys. Rev. B* **84**, 195437 (2011).
- [32] R. de Gail, M. O. Goerbig, F. Guinea, G. Montambaux, and A. H. Castro Neto, *Phys. Rev. B* **84**, 045436 (2011).
- [33] D. S. Lee, C. Riedl, T. Beringer, A. H. Castro Neto, K. von Klitzing, U. Starke, and J. H. Smet, *Phys. Rev. Lett.* **107**, 216602 (2011).
- [34] P. Moon and M. Koshino, *Phys. Rev. B* **85**, 195458 (2012).
- [35] V. I. Belinicher, A. L. Chernyshev, A. V. Dotsenko, and O. P. Sushkov, *Phys. Rev. B* **51**, 6076 (1995).
- [36] D. J. Scalapino, E. Loh, and J. E. Hirsch, *Phys. Rev. B* **35**, 6694 (1987).
- [37] G. Vignale and K. S. Singwi, *Phys. Rev. B* **39**, 2956 (1989).
- [38] G. Vignale and M. R. Hedayati, *Phys. Rev. B* **42**, 786 (1990).
- [39] C. Castellani, C. Di Castro, D. Feinberg, and J. Ranninger, *Phys. Rev. Lett.* **43**, 1957 (1979).
- [40] A. B. Harris and R. V. Lange, *Phys. Rev.* **157**, 295 (1967).
- [41] J. E. Hirsch, *Phys. Rev. Lett.* **54**, 1317 (1985).
- [42] A. H. Castro Neto, F. Guinea, N. M. R. Peres, K. S. Novoselov, and A. K. Geim, *Rev. Mod. Phys.* **81**, 109 (2009).
- [43] Q. L. He, L. Pan, A. L. Stern, E. C. Burks, X. Che, G. Yin, J. Wang, B. Lian, Q. Zhou, E. S. Choi, *et al.*, *Science* **357**, 294 (2017).
- [44] A. M. Black-Schaffer and K. Le Hur, *Phys. Rev. B* **92**, 140503(R) (2015).
- [45] A. M. Black-Schaffer and C. Honerkamp, *J. Phys.: Condens. Matter* **26**, 423201 (2014).
- [46] T. O. Wehling, E. Şaşıoğlu, C. Friedrich, A. I. Lichtenstein, M. I. Katsnelson, and S. Blügel, *Phys. Rev. Lett.* **106**, 236805 (2011).
- [47] H.-K. Tang, E. Laksono, J. N. B. Rodrigues, P. Sengupta, F. F. Assaad, and S. Adam, *Phys. Rev. Lett.* **115**, 186602 (2015).
- [48] N. N. T. Nam, and M. Koshino, *Phys. Rev. B* **96**, 075311 (2017).
- [49] F.-C. Zhang, C. Gros, T. M. Rice, and H. Shiba, *Supercond. Sci. Technol.* **1**, 36 (1988).
- [50] A. Abanov, A. V. Chubukov, and J. Schmalian, *Adv. Phys.* **52**, 119 (2003).